132
12/29/78

LA-7498-MS
Informal Report

DR. 2072

MASTER

Beam Tomography or ART in Accelerator Physics

University of California

LOS ALAMOS SCIENTIFIC LABORATORY
Post Office Box 1663 Los Alamos, New Mexico 87545

LA-7498-MS
Informal Report
UC-28
Issued: November 1978

Beam Tomography or ART in Accelerator Physics

John S. Fraser*

*Visiting Staff Member. Atomic Energy of Canada Limited, Physics Division, Accelerator Physics Branch, Chalk River Nuclear Laboratories, Chalk River, Ontario, Canada KOJ 1J0.

BEAM TOMOGRAPHY
or
ART IN ACCELERATOR PHYSICS

by

John S. Fraser

ABSTRACT

Projections of charged particle beam current density have been used for many years as a measure of beam position and size. The conventional practice of obtaining only two projections, usually in the horizontal and vertical planes, puts a severe limit on the detail that can be recovered from the projections. A third projection provides sufficient improvement to justify the addition of a wire to the conventional wire scanner in certain cases. A group of programs using algebraic reconstruction techniques was written to reconstruct beam current density from beam projections obtained at three or more specific or arbitrary angles around the beam. A generalized program, which makes use of arbitrary 2 × 2 transfer matrices between projections, can be used to reconstruct transverse or longitudinal emittance from appropriate projections. Reconstruction examples of beam current density and transverse and longitudinal emittance using experimental data from the Clinton P. Anderson Meson Physics Facility (LAMPF) accelerator beam are given.

I. INTRODUCTION

The techniques of three-dimensional reconstruction from projections (Computed Tomography or CT) have been applied for a number of years in electron microscopy and radiology. A comprehensive review of the algorithms used has been published by Gordon and Herman.[1] The most frequently used algorithm in the field of radiology is the two-dimensional Fourier transform method. A large number of projections (x-ray transmission profiles) at uniformly distributed angles around the subject are required by the complexity of the x-ray absorption pattern to be reconstructed.

In the field of accelerator physics, one expects that the relatively simple accelerator beam functions can be reconstructed from a smaller number of projections. For this purpose, the Algebraic Reconstruction Techniques (ART) introduced by Gordon, Bender, Herman, Lent, and Rowland[2-4] in 1970 are appropriate. The techniques show that increasing the number of projections or views equally spaced in a fixed angular range from as few as three to twenty causes very gradual improvement in the quality of the reconstruction. In other words, whereas a major improvement is made with three projections over two, additional projections add proportionally much less to the reconstruction quality. Criteria for the optimum choice of viewing angles in real space and in phase space are given in Appendix A.

For many years, projections of accelerator beam current densities have been used as a measure of beam diameter and position. The conventional practice of obtaining only two projections, usually in the horizontal and vertical planes, puts a severe limit on the amount of detailed information that can be recovered from the projections. The present work was undertaken to investigate the degree of enhancement to be gained by using three or more projections of beam current density. In 1969, Metzger[5] proposed the use of beam current density projections as a means of reconstructing the transverse phase space density of the beam. In Metzger's method, profiles are obtained at three locations in a drift space, with the central profile preferably taken at a beam waist. The three views in phase space correspond in a simple way to the several views in real space used in CT. A variant of Metzger's method has been described by Goodwin et al.[6] An evident advantage of this scheme over the conventional one for emittance measurements is that a wire scanner (or a nonintercepting beam profile measuring device) can be operated with a greatly reduced beam spill in or activation of the accelerator structure. In fact, for high-beam power applications, transverse beam emittance will probably be measurable only by reconstruction methods with nonintercepting profile measuring devices.

A natural extension of the method makes possible the reconstruction of the longitudinal phase space density from phase profiles. In this case, the beam current exceeding a given energy threshold is measured as a function of rf phase for three or more orientations of the bucket in phase space.

In both of the phase space applications of ART, a knowledge of the phase space transformation laws from one configuration to another is required. These correspond exactly to the real space rotational transformation between projection angles in CT.

II. THE ALGEBRAIC RECONSTRUCTION TECHNIQUE

The ART algorithms have a simple intuitive basis. Each projected density is thrown back across the reconstruction space in which the densities are repeatedly modified to bring each reconstructed projection into agreement with the measured projection. Comprehensive accounts of the ART algorithms have been published.[3,4] A brief review of the concepts will suffice for the present report.

We assume for this discussion that the pattern being reconstructed is enclosed in a square region. The reconstruction space is an $n \times n$ array of small squares called pixels. For each of the pixels, there is a grayness or density number, ρ_{ij}, which represents a uniform grayness over that pixel. A "ray" is a region of the space that lies between two parallel lines (see Fig. 1). The weighted ray sum is the total grayness of the digitized reconstruction figure within the ray. The projection at a given angle is then the set of ray sums in nonoverlapping, equally wide, parallel rays totally covering the figure.

The basic ART algorithm consists of altering the contents of each pixel intersected by the ray in such a way as to make the ray sum agree with the corresponding element of the measured projection. The alteration may be either an addition or a multiplication. When the next projection is encountered, the agreement with the previous projection is destroyed but as the iteration proceeds the mean deviation is reduced. The criterion for convergence commonly used for the additive ART[3] algorithm is the minimum variance, the variance being defined as

$$V(k) = \frac{1}{n^2} \sum_i \sum_j (\rho_{ij} - \bar{\rho})^2,$$

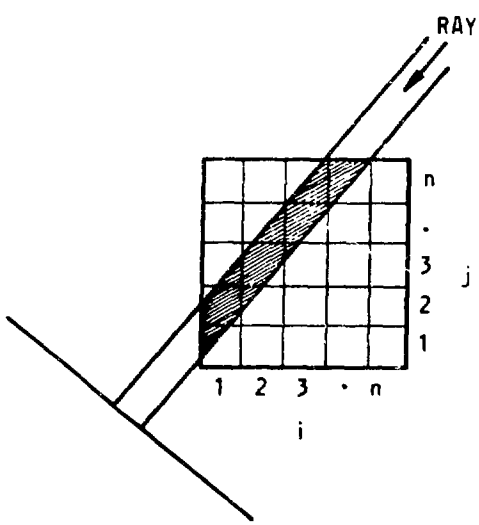

Fig. 1.
Reconstruction space of n^2 pixels.

where k is the iteration number, $\bar{\rho}$ is the mean density,

$$\bar{\rho} = \frac{1}{n^2} \sum_i \sum_j \rho_{ij},$$

and n^2 is the number of pixels in the reconstructed figure.

The true mean density can be obtained from the measured projections. If a projection vector p has n elements p_m then the mean density is

$$\bar{\rho} = \frac{1}{n^2} \sum_{m=1}^{n} p_m.$$

The multiplicative ART (MART) algorithm is equivalent to the maximum entropy solution.[7] The entropy of the reconstructed figure is defined as

$$H = \frac{1}{T} \sum_i \sum_j \rho_{ij} \ln \frac{\rho_{ij}}{T},$$

where $T = \sum_i \sum_j \rho_{ij}$ is the total density.

Tests carried out using pseudoprojection data and experimental data with several two- and three-view reconstructions (see Sec. III) show that convergence criteria based on the residual errors in the projection data are more reliable.[7] The minimum variance criterion is not suitable for the highly peaked beam current and phase space densities encountered in accelerator physics. If P_m^q is the mth ray sum for a given projection angle after the qth iteration, the mean square error is

$$\epsilon_p^q = \sum_{m=1}^{n} (p_m^q - p_m)^2/n.$$

The iteration is terminated if any $\epsilon_p^{q+1} > \epsilon_p^q$ after at least three iterations have been completed.

III. COMPUTER CODES

The wire scanners used in the Clinton P. Anderson Meson Physics Facility (LAMPF) are each equipped with a horizontal and a vertical wire. As part of an experimental study of accelerator beam core modeling, three additional wires were added at −15°, 45°, and 105° from the horizontal. In addition to the usual perpendicular views, projection data from the five wires were combined in two groups of three views, one with 45° intervals and the other with 60° intervals. Computer codes based on the MART algorithm subroutine[7] were developed to reconstruct the accelerator beam current density. A generalized version of the code, RECON, was written to use with any system in which the reconstruction space may be transformed from one projection configuration to another by a 2-by-2 matrix transformation. It is thus suitable for the reconstruction of phase space diagrams from beam current or phase profiles. Beam current density can also be reconstructed with the generalized RECON code because the 2-by-2 transformation involved is just the rotation transformation,

$$R = \begin{bmatrix} \cos\theta & \sin\theta \\ -\sin\theta & \cos\theta \end{bmatrix}.$$

A. Profile Preparation and Display of Results

The convention adopted in the present group of programs is a profile length of 51 elements. The corresponding reconstruction space is a 51-by-51 element matrix. The odd number of row and column elements is used because it is convenient to rotate the contents of the array about the center of a pixel rather than about an intersection of pixel boundaries.

The profiles must be normalized to the same total area. This is dictated by the MART algorithm, which compares ray sums taken in various directions across the same space with the corresponding measured data. The total areas under computed profiles will thus all be the same.

The ordering of the elements of the profiles must conform to the convention of the program being used. In two of the specialized programs, RECON60 and RECON45, specific directions are assumed for the projections and, furthermore, a specific sequence for the projection elements is also assumed. Details of the convention are given in Appendix B. The more general programs, RECONWT and RECON, can accommodate any ordering through the choice of the appropriate rotation angles or transformation matrices.

When more than two profiles are being used in a reconstruction, all but two profiles must be shifted if

there is an inconsistency in the centers of gravity of the profiles. The projection in a given direction of the center of gravity of a function of two variables coincides with the center of gravity of the projection of the function. Therefore, the back projection of the centers of gravity of the profiles must intersect at the center of gravity of the function. Thus, even though the position of the center of gravity of the reconstructed density may not be important, it is essential for consistency to make all but a given two profiles conform to the location of the center of gravity defined by the back projection of the given two profiles.

A group of programs, PREP360, PREP345, etc., were written to carry out the profile manipulations described above.

When the reconstruction is completed, certain operations may have to be done on the matrix to make it conform to the exigencies of line printers and graphic display packages. For printing out the matrix, for example, it is convenient to have the horizontal direction parallel to the printed line or matrix row. If, during the iteration sequence in the reconstruction, the horizontal direction in space did not correspond to the matrix row, the contents of the matrix should be rotated to make the result more readily intelligible.

In addition to printing out the numerical values of the pixels, a 37-gray level[8] representation was included in the programs, providing a means of rapid assessment of the shape and orientation of the reconstructed figure on line printer output. More detail is usually apparent in contour plots or three-dimensional plots. (See Sec. IV.)

B. RECON60

This program uses the hexagonal grid and the MART reconstruction subroutine described by *Minerbo and Sanderson*,[7] which is designed specifically for beam current density profiles taken with wires spaced 60° apart. With the correct ordering of the profiles (see Appendix B), the three views can be considered to be equally spaced around the beam at 120° intervals.

The hexagonal reconstruction grid is represented internally in a two-dimensional matrix. (See Fig. 2.) Before the reconstructed current density can be conveniently displayed, the hexagonal grid must be mapped onto a rectangular grid. Let L, M be the indices for the equilateral triangular pixels in the hexagonal grid. We assume the center element, L = M = 26, will be mapped to the center of a square grid

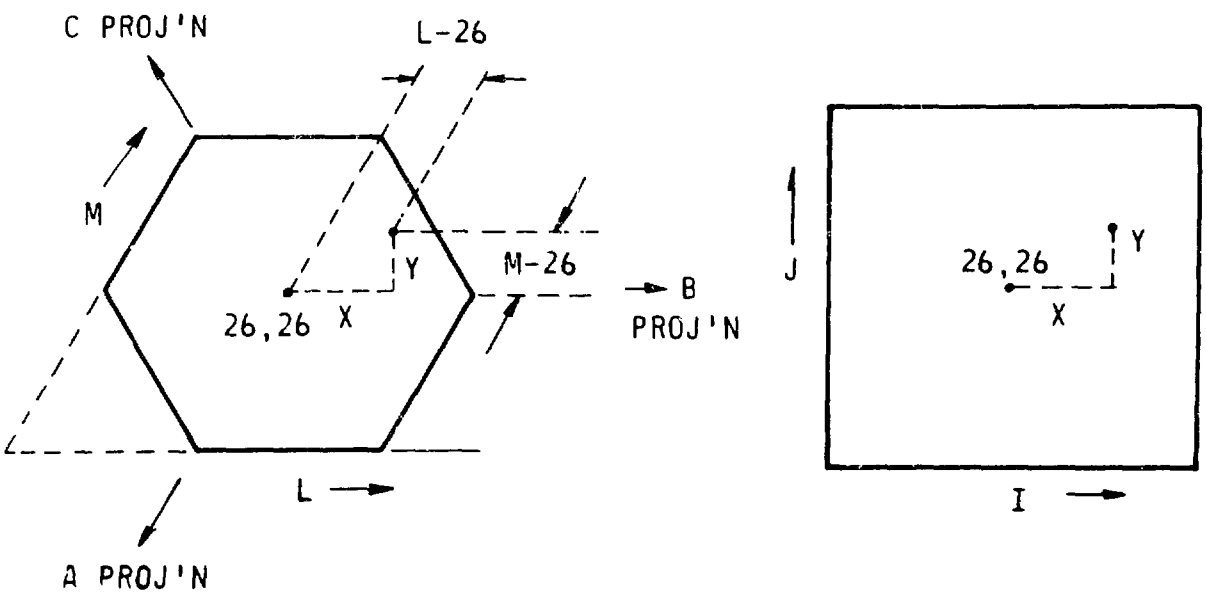

Fig. 2.
A hexagonal grid mapped onto a square grid.

with indices I = J = 26. The horizontal and vertical displacement of a pixel in the hexagonal grid are then X = L−26 + (M−26) cos 60°, Y = (M−26) sin 60°. The same displacements in the rectangular grid are X = I−26, Y = J−26.

Following the mapping operation, the reconstructed figure may have to be rotated as described above if the B projection plane does not correspond to the vertical.

Details of the MART subroutine, which is the basis of this program and from which the other programs described here were derived, may be found in Ref. 7.

C. RECON45

For the LAMPF wire scanners, which are normally equipped with a horizontal and a vertical wire, the simplest conversion to permit three profiles of the beam to be taken is the addition of one wire at 45°, bisecting the angle between the original two wires. A special reconstruction grid was devised for this geometry, which allows ray sums for all three views to be done without weighting (see Appendix C). The use of unweighted summations requires that the wire scanner step size for the 45° view be $1/\sqrt{2}$ times that for the horizontal and vertical views. For the 45° view, the projected step size is equal to the actual step size. To allow for the fact that the projected step sizes for the usual two views are $1/\sqrt{2}$ times the actual step size (Appendix B), the operational computer control programs multiplies the requested projected stroke length (100 steps) by $\sqrt{2}$ to determine the actual stroke length. Thus, for the three views at 45° intervals the requested stroke for the intermediate view at 45° must be 1/2 that for the other two.

Rotation of the reconstructed figure is not required in RECON45 but correct ordering of the measured profiles is essential (Appendix B).

C. RECONWT

This program was written to accommodate arbitrary angles between profiles. In the present version of the program, two to four profiles can be used. Extension to larger number of profiles is straightforward.

As noted by Herman et al.,[3] the use of weights in the pixels intersected by the projected rays greatly increases not only the computing time but also the memory requirements. In unweighted ART, the pixel weight is unity if the center of the pixel is within the ray and zero if outside. In weighted ART the fractional area of each pixel enclosed in the ray is used. The fractional areas must be computed for each ray; for each profile of m elements, the number of weights required for n^2 pixels is $m \times n^2$. Most of the weights are, of course, zero.

In RECONWT, only the nonzero weights are retained. For each projection, four vectors are calculated and stored on a disk file. During the iterative reconstruction, only the vectors for the current projection are retained in core. The four vectors are

1. the number L of the intersected pixels for each of the m profile elements,
2. the row indices and
3. the column indices for L pixels, and
4. the weights or fractional areas of the intersected pixels.

The details of the weight calculation can be found in Appendix D.

In RECONWT, profile ordering is not mandatory but the angle specified in the weights calculation must correspond to the actual ordering of the measured data. RECONWT is clearly much slower than the unweighted, but specialized, programs RECON60 and RECON45. It is, however, more flexible and can readily be modified to handle more than four views.

E. RECON

In contrast to the three programs just described for reconstruction from profiles measured at various angles in real space, the last program in this group, RECON, was generalized to use any 2-by-2 transformation matrix between projections. The rotation transformation is a special case of the general 2-by-2 matrix transformation.

In RECON, the ray sums are column sums in the reconstruction matrix. In going from one projection to another, the reconstruction space is mapped from the first configuration to the second. Reconstructions from projections from phase space under varying conditions can readily be carried out, provided

the transformation laws are known. Transverse emittance diagrams can be reconstructed from beam current profiles taken at three locations in a drift space or, alternatively, from one location with three different settings of the upstream beam transport or accelerator parameters. In each case the transfer matrices would have to be known from measurement or an auxiliary calculation. In a similar way, the longitudinal emittance may generally be reconstructed if the energy or phase profiles can be measured under three or more sets of conditions. Again, the transfer matrices must be known

The current version of the program uses three profiles but only two transfer matrices are required. If the profiles are measured in configurations 1, 2, and 3, the transfer matrices between 1 and 2 and between 2 and 3 must be supplied and the third is calculated by RECON. To ensure that after each iteration cycle the reconstruction space is restored, we require that the transfer matrices R_{ij} satisfy the matrix product.

$$R_{31}R_{23}R_{12} = 1,$$

where 1 is the unit matrix.

The useful part of the reconstruction space is the part of the n × n matrix that remains within the matrix through all of the transformation steps. Consequently, the three mappings, R_{12}, R_{23}, and R_{31} are applied to the space, and only the surviving pixels are used in subsequent calculations. Each surviving pixel starts out with the mean density $\bar{\rho}$.

Provision is made for a final transformation after the iteration cycles are completed to orient the reconstructed figure for display.

The linear transformations represented by the transfer matrices transform a square pixel into a quadrilateral. In the mapping procedure the contents of the old pixel must be distributed among all of the new pixels overlapped by the quadrilateral. Appendix E contains a discussion of the subroutines developed for mapping under linear transformations.

IV. RECONSTRUCTION EXAMPLES

A. Test Figures

It is instructive to test the reconstruction capabilities of the codes with two to four views by using pseudoprojections from known test figures. Five easily generated figures were chosen: hollow and solid cylinders, a single and a pair of two-dimensional gaussians, and a cone.

In Fig. 3 these five test figures are shown with reconstructions from two profiles 90° apart, three profiles 45° apart, and three profiles 120° apart. Clearly, reconstruction from two views 90° apart is sensitive to the generation of artifacts; from the hollow cylinder profiles, four symmetrically spaced peaks appear; and from the profiles for two gaussians on a line bisecting the angle between the projection planes, again four peaks are produced. The cone and single gaussian are reproduced well but the solid cylinder reconstruction, although symmetrical, fails to reproduce the sharp discontinuity in the density at the surface.

Three views 45° apart are an improvement over two views 90° apart, but the hollow and solid cylinders are still poorly reproduced. However, the additional view removes the two false peaks from the reconstruction of two gaussians.

Further improvement is obtained with three views if the angle between adjacent views is increased to 120°. The cylinders, both solid and hollow, are more symmetrical than in the previous examples and the sharp density discontinuity is quite well reproduced.

These examples verify qualitatively the criterion stated by Crowther et al.;[9] that is, the projection angles should be distributed uniformly around the test object for the most faithful reconstruction. The examples also show axially symmetric objects without sharp discontinuities can be fairly well reconstructed from only two profiles 90° apart. Three views, especially if they are at the angular spacing of 120°, are a great improvement. In particular, the three-view system is probably capable of

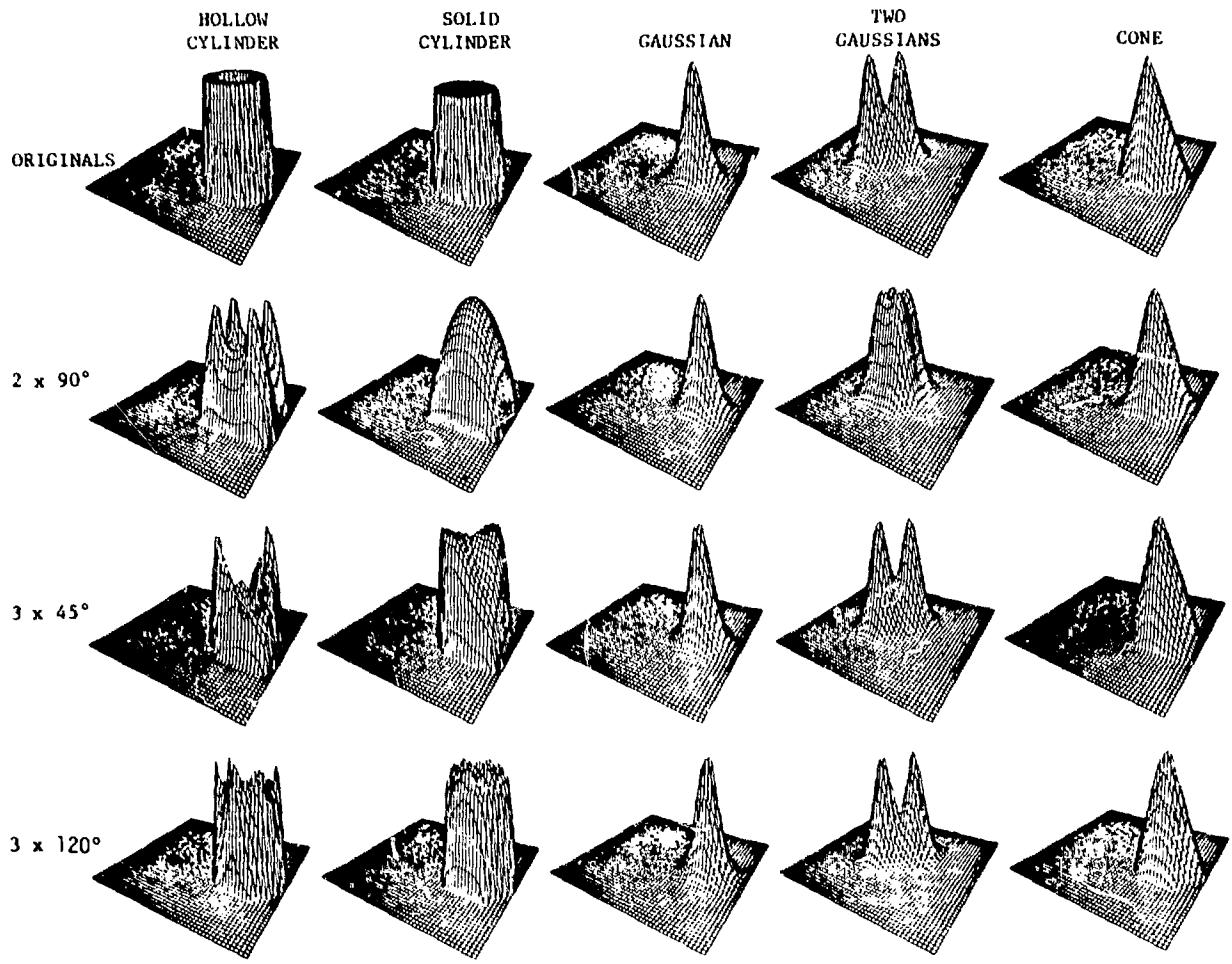

Fig. 3.
Test figures and reconstructions using two views 90° apart and three views 45° and 120° apart.

reconstructing profile sources in accelerator physics such as beam current and phase space density with the proviso that the structure in the profiles is not too complicated.

B. Beam Current Density

As part of a program to improve our understanding of the beam behavior in the LAMPF accelerator, a wire scanner was modified by the addition of three wires to the conventional horizontal and vertical wires (see Fig. B-1 in Appendix B). A wire at 45° to the horizontal permitted three views 45° apart to be taken. Additional wires were placed at −15° and 105°. When these two are used with the 45° wire and with the appropriate profile ordering, three views spaced 120° apart can be obtained.

The modified wire scanner was located in the transition region between the 201.25-MHz drift tube linac and the 805-MHz coupled cavity linac. Profiles were recorded on each wire separately while all other wires were grounded. The beam pulse repetition rate was reduced to 7.5 Hz and the peak current was 5 mA. Each profile was recorded in 100 steps, one set of five with a constant actual step size, and a second set with a constant projected step size. A quadrupole doublet 1.5 m upstream from the wire

scanner was turned on and off, profiles being recorded under both conditions.

Reconstructions of the beam current density from this data are shown in Figs. 4 to 8. In Fig. 4, the doublet was off and in Fig. 5 it was on. The contour diagram in Fig. 4 shows that the core of the beam is essentially circular. In Fig. 5, with the doublet turned on, the beam is elongated in the vertical plane. The three-dimensional plots are smooth, as is to be expected from the lack of structure in the profiles.

When three views are taken of the same beam, as shown in Figs. 6 to 9, a small horizontal-vertical correlation is revealed. In Figs. 6 and 7, three views 45° apart are used and in Figs. 8 and 9, three views 120° apart are used. In contrast to the poorer performance of the 45° system with the more demanding of the test figures, the more regular features of the beam current density are reconstructed by the 45° system equally well as by the 120° system. In Figs. 4 to 7, the beam reconstructions are apparently larger than in Figs. 8 and 9 because the reconstruction pixel width corresponds to 0.42 mm in the former group and to 0.59 mm in the latter pair of figures. Figure 10 is a 37-level gray scale[8] line printer rendition of the beam shown in Fig. 9.

An attempt was made to reproduce settings of the linac parameters that had previously produced double-humped vertical and/or horizontal beam profiles. It was not possible to do so, probably because the ion source and column operating conditions had been changed significantly since the earlier measurements. Prominent shoulders were produced on the vertical profile, however, and the three-dimensional current distribution derived from three profiles 45° apart is shown in Fig. 11. Certainly, a double-beam-feature would have been clearly reconstructed much like that of the two-gaussian test figure discussed in an earlier section.

C. Transverse Emittance

Horizontal and vertical beam profiles were recorded at the end of Module 1 of the drift tube linac while the Module 1 quadrupole currents were varied from 80% to 104% of the nominal operating currents. Three profiles were selected that best fit Metzger's criteria[5] (see Appendix A). Transfer matrices for the vertical and horizontal planes were calculated for the beginning to the end of Module 1 using PARMILA.

If the transfer matrices from the Module 1 entrance configuration of the beam under the three chosen conditions are R_1, R_2, and R_3, the transfer matrices required to transform the reconstruction phase space from one profile configuration to another are R_{12} and R_{23}, as shown in Fig. 12. Since $R_2 = R_{12}R_1$ and $R_3 = R_{23}R_2$, then R_{12} and R_{23} can be obtained from the PARMILA results by the relations

$$R_{12} = R_2 R_1^{-1}$$

and

$$R_{23} = R_3 R_2^{-1}.$$

The transverse emittances reconstructed from the profiles are shown in Figs. 13 and 14. The normalized emittances obtained with a threshold of 6% of the peak are 0.071 π cm-mrad and 0.054 π cm-mrad for the horizontal and vertical, respectively. When compared with the normalized emittances measured at the entrance to Module 1 (EM-3 device) of 0.020 π cm-mrad and 0.011 π cm-mrad, emittance growths of factors between 3 and 5 are indicated.

An estimate of the projection angles for the three views in the normalized horizontal emittance plane was made by transforming an unmatched ellipse from the unnormalized to the normalized phase space coordinates (see Appendix A). The results were 98° for R_{12} and 58° for R_{23}. These are both well below the Metzger criteria but are probably adequate, in view of the relatively good quality of reconstruction of smooth test figures with the 45° system.

D. Longitudinal Emittance

In the longitudinal plane, projections of the phase space can be made either onto the energy axis or onto the phase axis. The phase scan method[9] provides a convenient means of obtaining phase profiles at certain locations in the linac. Phase profiles were measured at the end of Module 5 with the rf field level in Module 5 set at 98%, 100%, and 102% of the design value. The matrices connecting

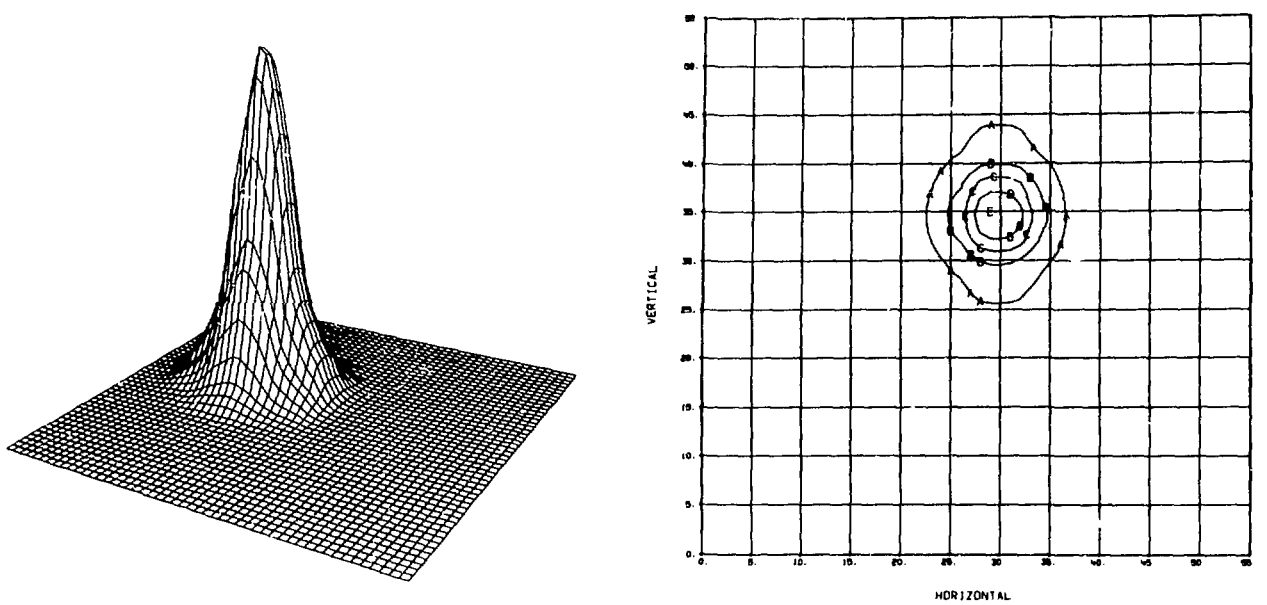

Fig. 4.
Three-dimensional and contour diagrams of beam current reconstruction from two profiles 90° apart.

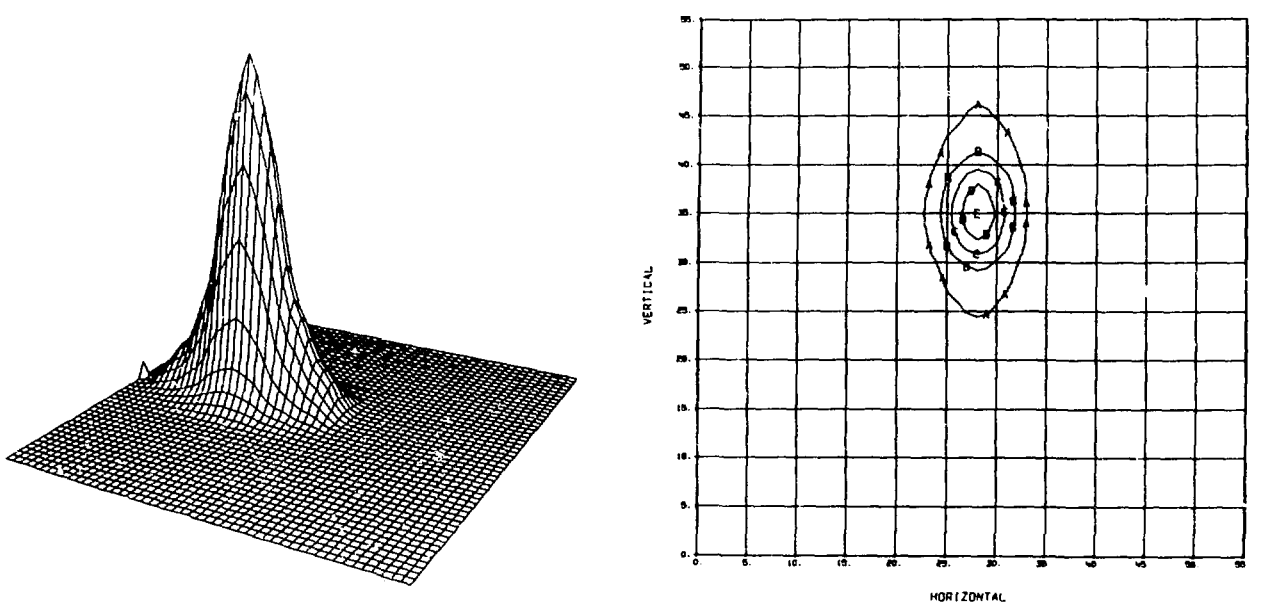

Fig. 5.
As in Fig. 4 but with a quadrupole doublet immediately before the wire scanner turned on.

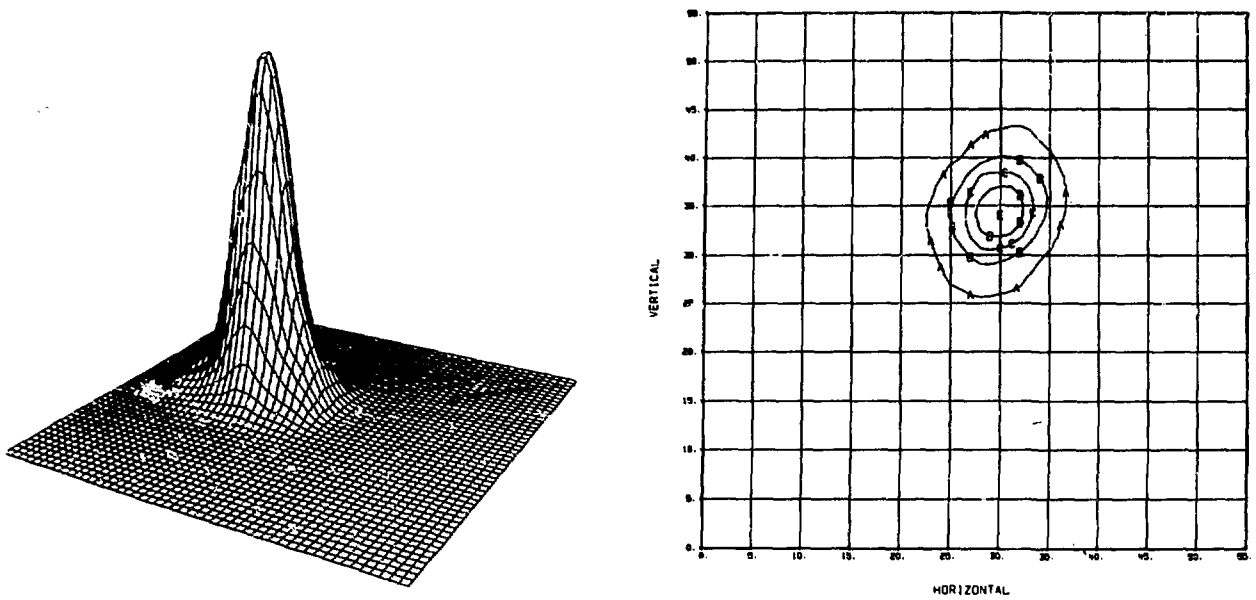

Fig. 6.
As in Fig. 4 but reconstructed from three profiles 45° apart.

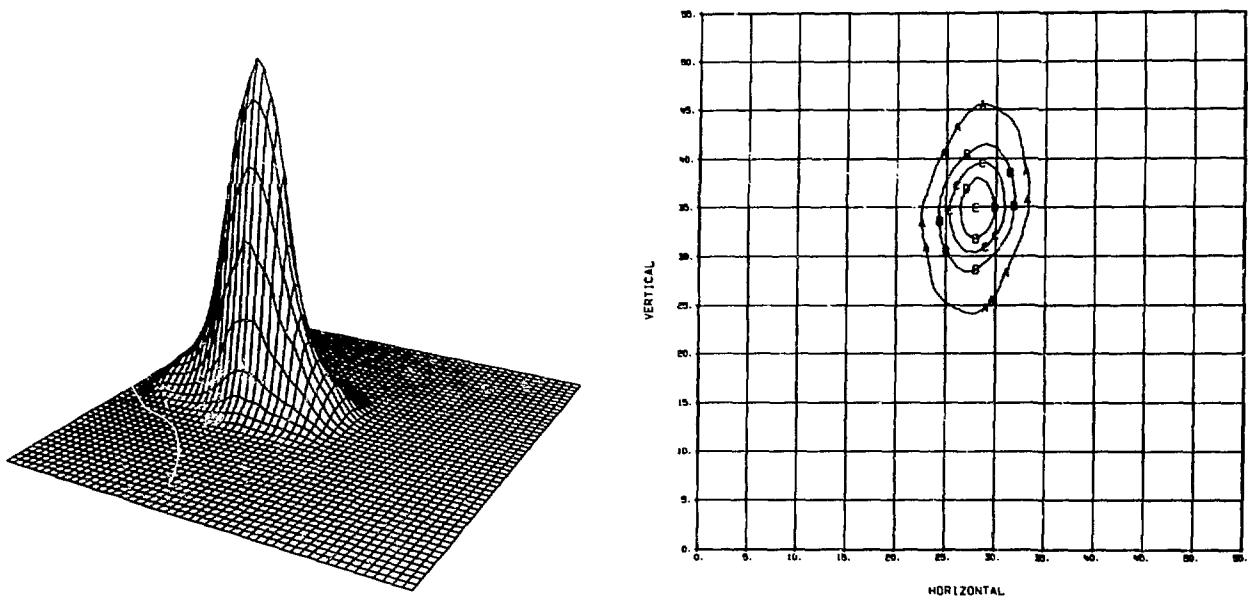

Fig. 7.
As in Fig. 5 but reconstructed from three profiles 45° apart.

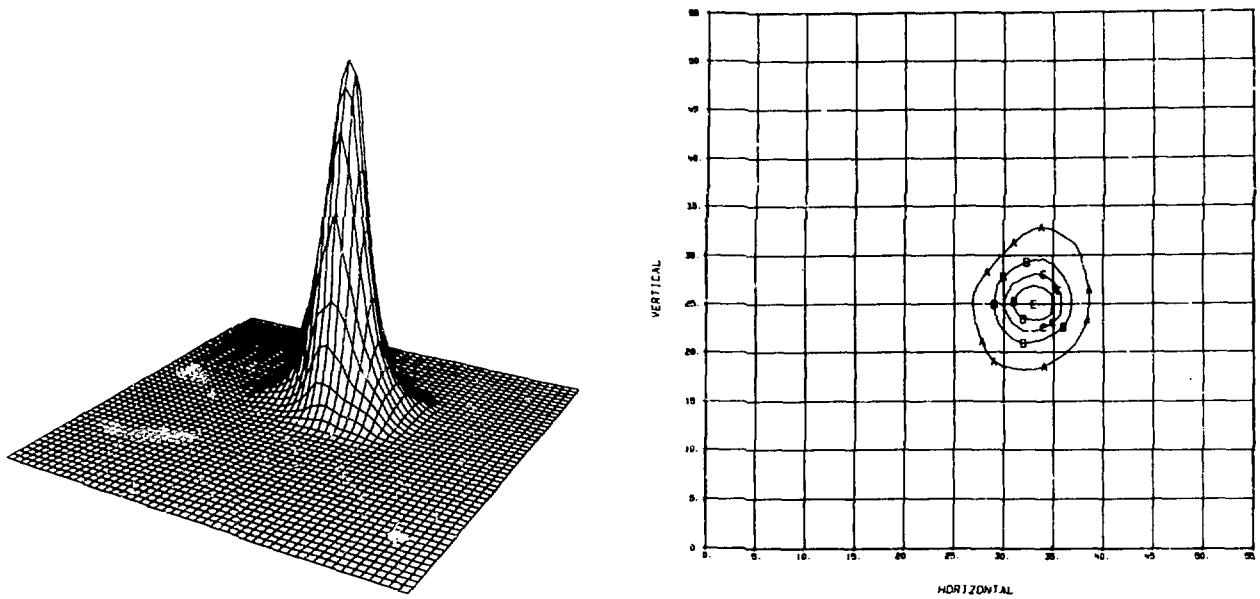

Fig. 8.
As in Fig. 4 but reconstructed from three profiles 120° apart.

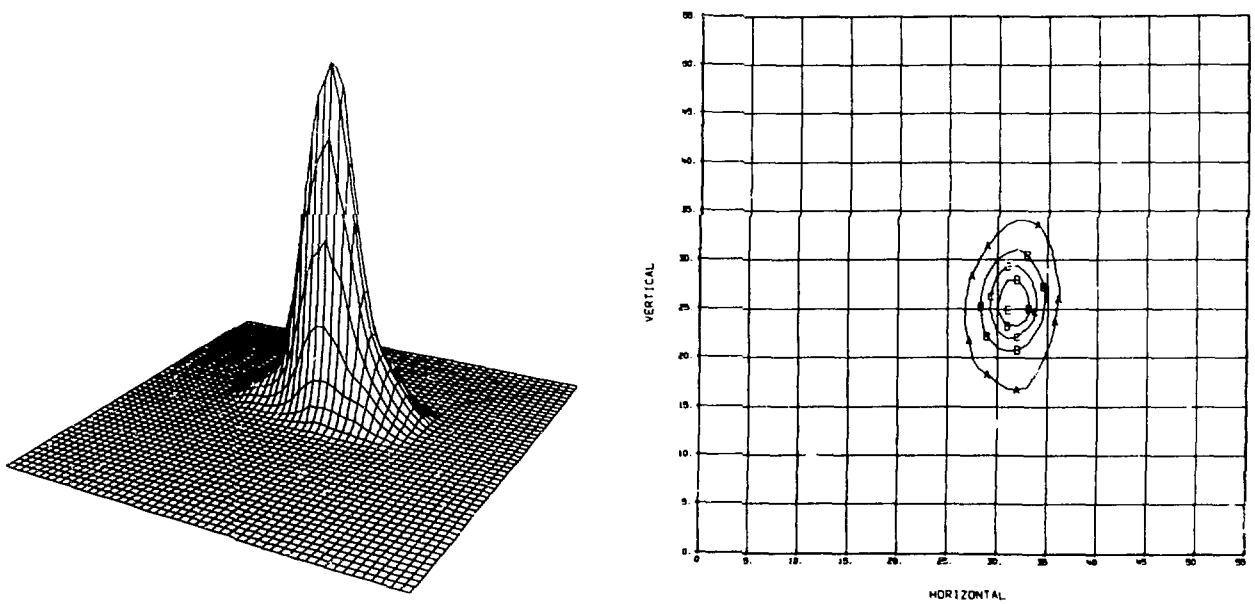

Fig. 9.
As in Fig. 5 but reconstructed from three profiles 120° apart.

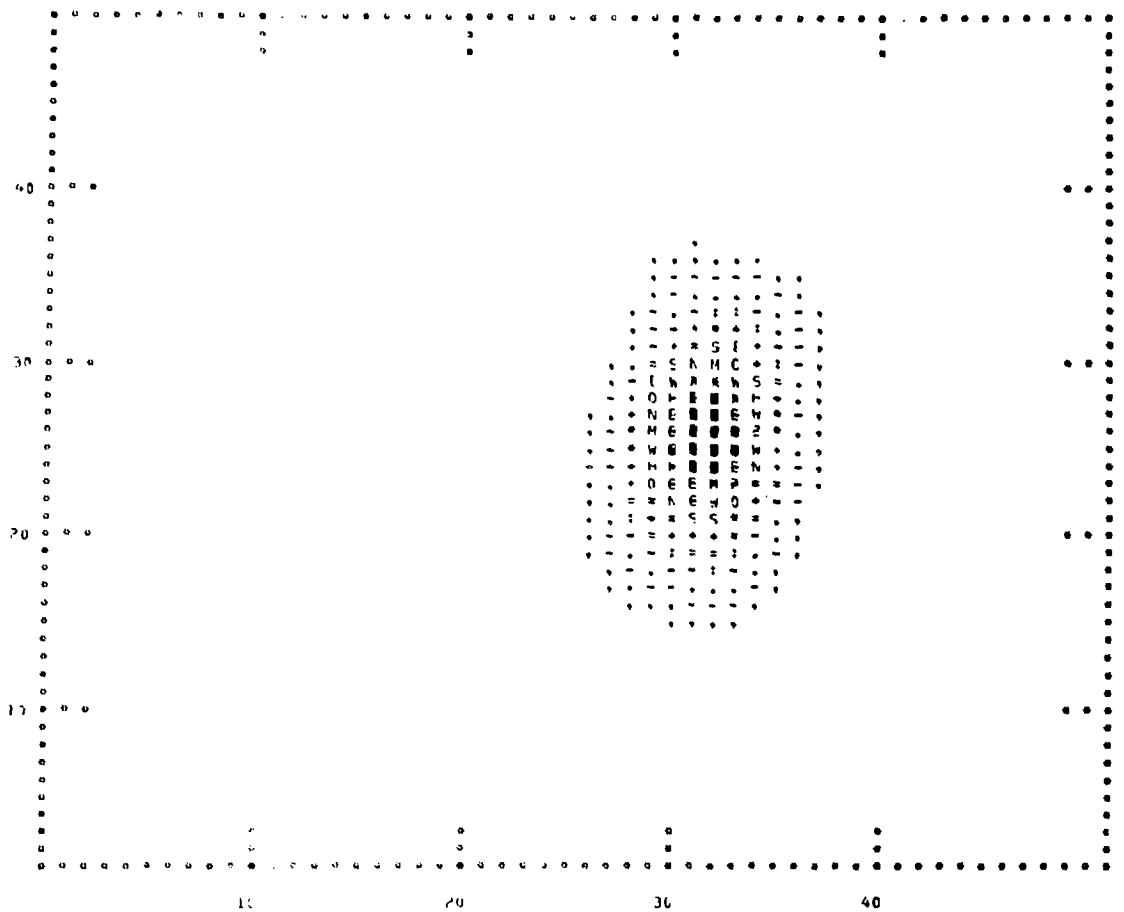

Fig. 10.
A 37-level gray scale line printer display of the beam current density reconstruction shown in Fig. 9.

the three longitudinal phase space configurations were obtained from PARMILA calculations by the method outlined in the previous section.

Phase profiles measured for an unoptimized beam and for an optimized beam are shown in Fig. 15. The longitudinal emittance of the unoptimized beam obtained with the RECON code is shown in Fig. 16 and for the optimized beam in Fig. 17. The emittances calculated using a 6% threshold are 0.89 π MeV·deg and 0.34 π MeV·deg, respectively (the degrees refer to the phase in the 201.25-MHz rf period). The three-dimensional plot of the optimized beam shows a smoother, more compact distribution than does the plot for the unoptimized beam. The half-widths of the optimized beam phase space as deduced from the fitted ellipse constants are

$$\sqrt{\frac{\gamma\varepsilon}{\pi}} = 0.13 \text{ MeV}$$

and

$$\sqrt{\frac{\beta\varepsilon}{\pi}} = 3.4 \text{ deg.}$$

No independent determinations of these quantities exist but they are plausible values.

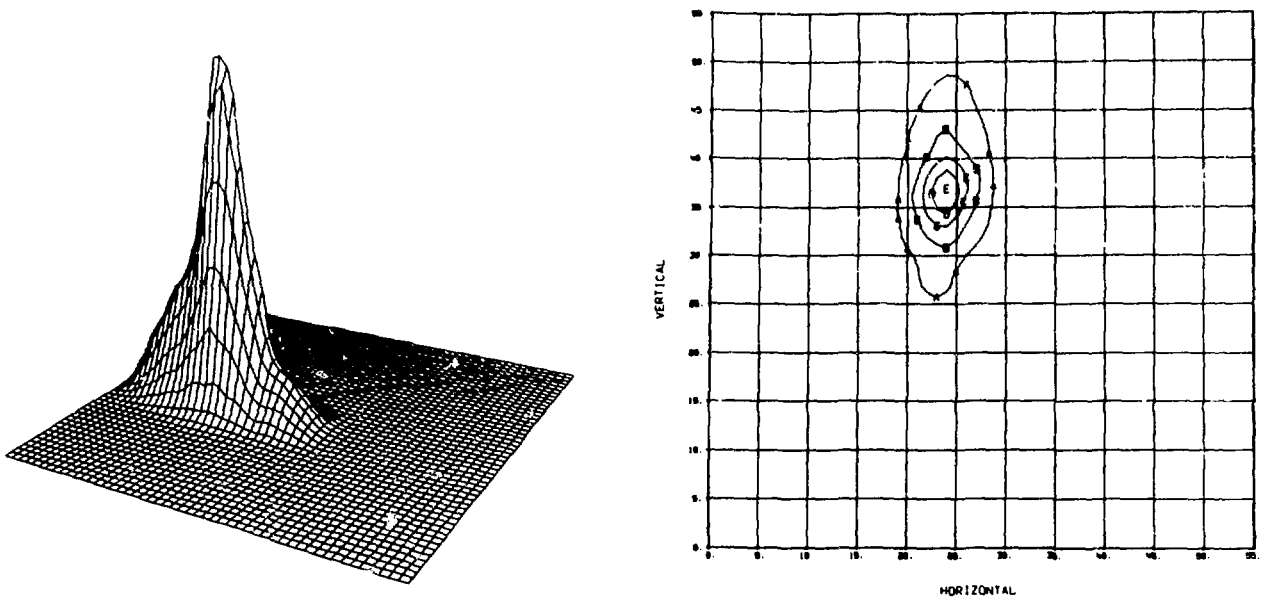

Fig. 11.
A poorly tuned beam reconstructed from three profiles 45° apart.

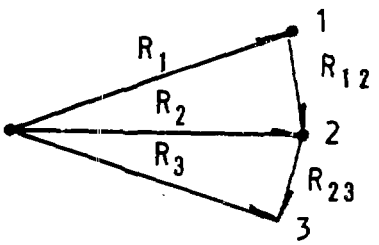

Fig. 12.
Schematic representation of matrices connecting an entrance configuration of a beam with three different exit configurations.

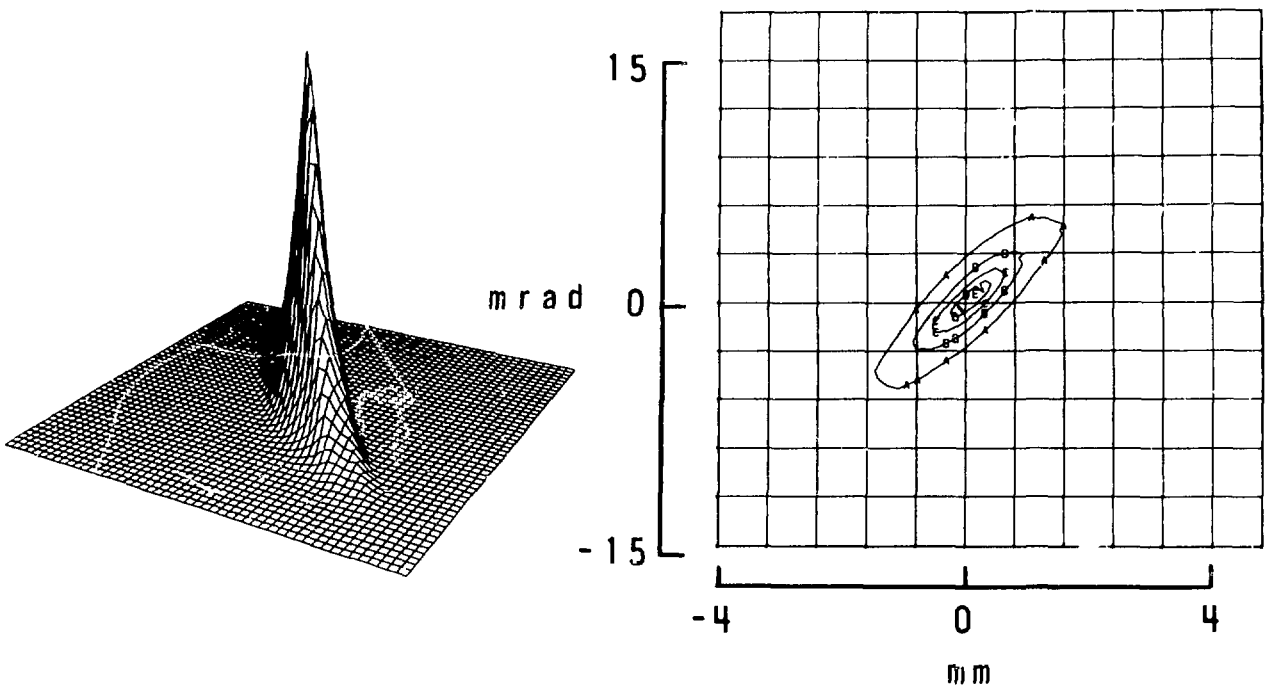

Fig. 13.
Vertical emittance of the beam at the exit of Module 1 reconstructed from three beam current profiles taken with Module 1 quadrupole settings 80%, 96%, and 104% of the nominal value.

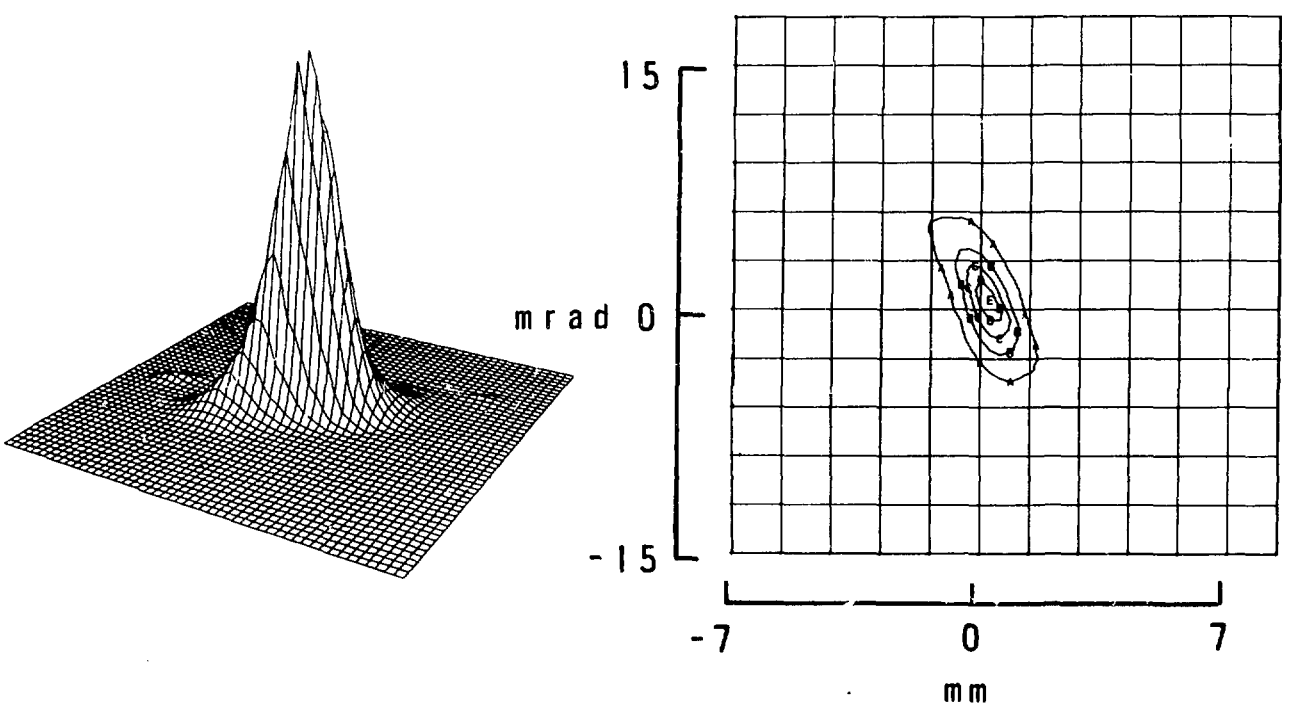

Fig. 14.
Horizontal emittance at the exit of Module 1 under the conditions given in Fig. 12.

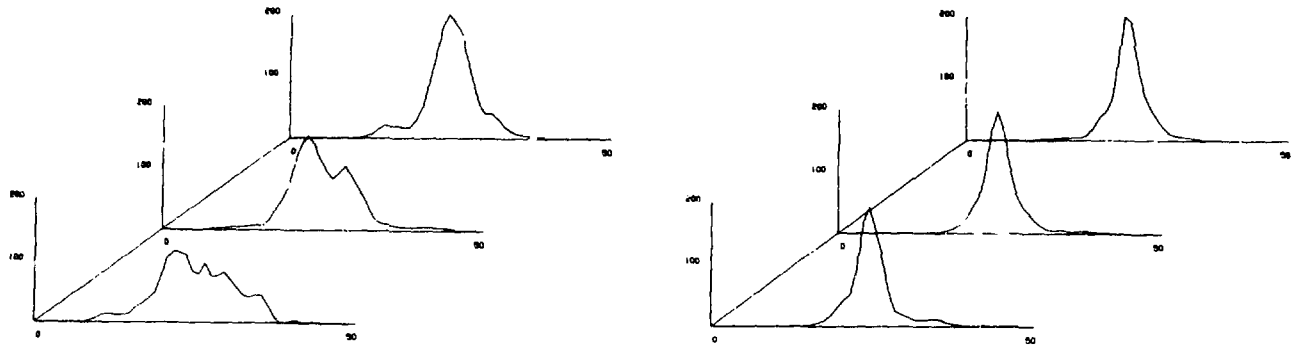

Fig. 15.
Phase profiles at the end of Module 5 measured for an unoptimized beam (left) and an optimized beam (right). The field amplitudes were 98%, 100%, and 102% of the nominal value.

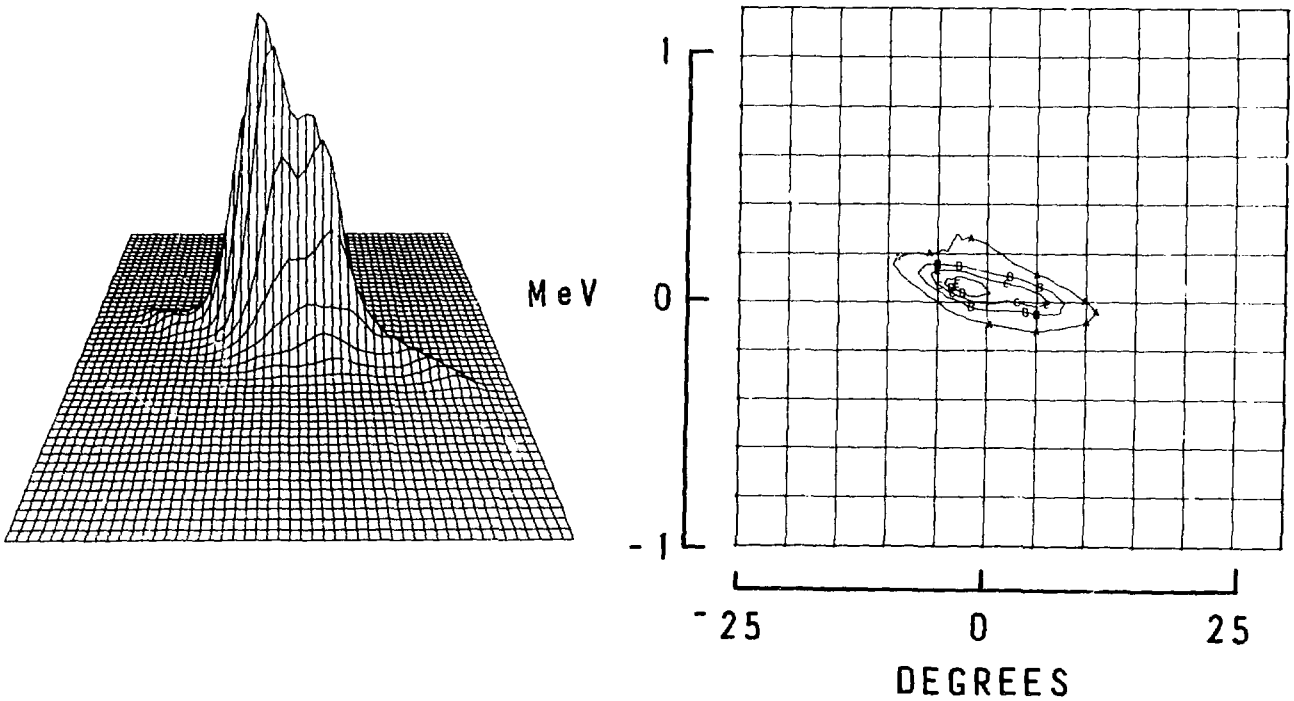

Fig. 16.
Longitudinal emittance of an unoptimized beam reconstructed from phase profiles with the rf field amplitude in Module 5 at 89%, 100%, and 102% of the nominal value.

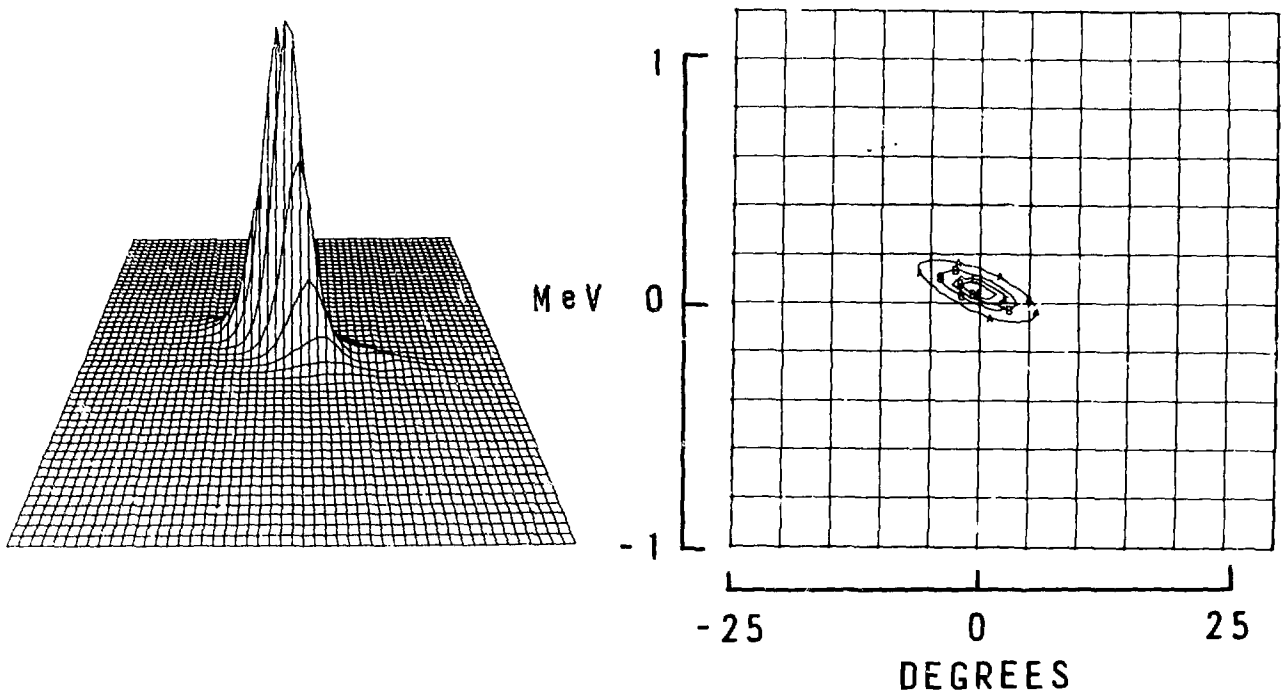

Fig. 17.
Longitudinal emittance of an optimized beam reconstructed from phase profiles under the conditions of Fig. 16.

ACKNOWLEDGMENTS

I am indebted to Oscar Sander of LASL Group MP-9 for the wire scanner modification and for the beam profile data used in the beam current density reconstruction. I am indebted to Andrew Browman for the beam profiles obtained from a wire scanner at the end of Module 1. I am indebted to Rene Mills for carrying out the PARMILA calculations. I thank Ken Crandall for the Module 5 phase scan data and for the associated PARMILA calculations of the longitudinal transfer matrices.

REFERENCES

1. R. Gordon and G. T. Herman, "Three-Dimensional Reconstruction from Projections: A Review of Algorithms," Int. Rev. Cytol. **38**, 111 (1974).

2. R. Gordon, R. Bender, and G. T. Herman, "Algebraic Reconstruction Techniques (ART) for Three-Dimensional Electron Microscopy and X-Ray Photography," J. Theor. Biol. **29**, 471 (1970).

3. G. T. Herman, A. Lent, and S. W. Rowland, "ART: Mathematics and Applications," J. Theor. Biol. **42**, 1 (1973).

4. R. Gordan, "A Tutorial on ART," IEEE Trans. Nucl. Sci. **NS-21**, 78 (June 1974).

5. C. Metzger, "Measurement of Beam Emittances and Beam Centering in the 800 MeV Measurement Line of the P.S. Booster," CERN/SI/Int. DL/69-10 (1969) and G. Bariband and C. Metzger, "The 800 MeV Measurement Line of the CERN P.S. Booster," IEEE Trans. Nucl. Sci. **NS-20**, No. 3, 659 (June 1973).

6. R. W. Goodwin, E. R. Gray, G. M. Lee, and M. F. Shea, "Beam Diagnostics for the NAL 200-MeV Linac," Proc. 1970 Prot. Lin. Accel. Conf., FNAL (1970) p. 107.

7. G. N. Minerbo and J. G. Sanderson, "Reconstruction of a Source from a Few (2 or 3) Projections," Los Alamos Scientific Laboratory report LA-6747-MS (1977).

8. P. Henderson and S. Tanimoto, "Considerations for Efficient Picture Output via Lineprinter," Comput. Graphics and Im. Proc. 3, 327 (1974).

9. R. A. Crowther, D. J. DeRosier, and A. Klug, "The Reconstruction of a Three-Dimensional Structure from Projections and Its Application to Electron Microscopy," Proc. Roy. Soc. London, Ser. A 317, 319 (1970).

10. R. A. Jameson, W. E. Jule, R. S. Mills, E. D. Bush, Jr., and R. L. Gluckstern, "Longitudinal Tuning of the LAMPF 201.25-MHz Linac Without Space Charge," Los Alamos Scientific Laboratory report LA-6663 (March 1978).

11. J. Guyard and M. Weiss, "Use of Emittance Measurements in Matching Problems," Proc. 1976 Prot. Lin. Accel. Conf., Atomic Energy of Canada Limited, report no. AECL-5677, 254 (1976).

12. E. D. Courant and H. S. Snyder, "Theory of the Alternating-Gradient Synchrotron," Ann. Phys. (NY) 3, 1 (1958).

13. K. L. Brown, B. K. Kear, and S. K. Howry, "TRANSPORT/360," Stanford Linear Accelerator Center report SLAC-91.

APPENDIX A

CRITERIA FOR OPTIMUM CHOICE OF VIEWING ANGLES

In CT, projection angles uniformly distributed around the test object result in the most faithful reconstruction.[10] This has been verified with pseudoprojection data from a bivariate Gaussian distribution with a major-to-minor axis ratio of 8. The most unfavorable orientation of the figure is with the major axis parallel to one projection plane. Two cases were tested. In one, three views at 0°, 45°, and 90° were used (RECON45). In the other, three equally spaced views around the figure were used (RECON60). In both cases, convergence was slow but RECON60 converged more rapidly. The angle of orientation was determined within two or three iterations in both programs. The major axis was also determined rapidly but the minor axis (normal to one projection plane) was initially overestimated and converged slowly but monotonically toward the correct value.

The equal spacing of three views has been carried over from real space to phase space by Metzger.[5] In normalized transverse phase space, the beam is contained within a circle of radius $\sqrt{\epsilon/\pi}$, where ϵ is the emittance. The transformation from unnormalized coordinates y, y' to normalized coordinates η, η' is given by[11]

$$\begin{bmatrix} \eta \\ \eta' \end{bmatrix} = \begin{bmatrix} \frac{1}{\sqrt{\beta}} & 0 \\ \frac{\alpha}{\sqrt{\beta}} & \sqrt{\beta} \end{bmatrix} \begin{bmatrix} y \\ y' \end{bmatrix}$$

and

$$\beta\gamma - \alpha^2 = 1,$$

where α, β, and γ are the beam ellipse parameters[12] in the equation

$$\gamma y^2 + 2\alpha y y' + \beta y'^2 = \epsilon/\pi.$$

The combined beam ellipse transformation through a point-to-point transformation (R) and to normalized phase space coordinates (N) is given by

$$\sigma_N = (NR)\,\sigma_o\,(NR)^T .$$

Three equally spaced views of the circle in normalized phase space are shown in Fig. A-1. The tangent rays P_1P_3 and P_2P_3 make angles of 30° and 150° with the η axis so the intercepts are at a distance.

$$OP_1 = OP_2 = \eta_1 = 2\sqrt{\varepsilon/\pi}$$

from the origin.

The three views shown are 120° apart. If the viewing direction 2 were reversed, the projection would be identical, provided that due account was taken of the ordering of the profile (Appendix B). In this case, the three views are 60° apart.

Consider the special case of a beam in a drift space with a waist at position 2. In unnormalized phase space the intercept corresponding to P_3 is y_1, where

$$\eta_1 = \frac{y_1}{\sqrt{\beta}} = y_1\sqrt{\gamma} = 2\sqrt{\varepsilon/\pi} ,$$

$$\therefore y_1 = 2\sqrt{\varepsilon/\gamma\pi} = 2\sqrt{\sigma_{11}} ,$$

and where $\sqrt{\sigma_{11}}$ is the maximum extent of the beam ellipse at the waist in TRANSPORT[18] notation.

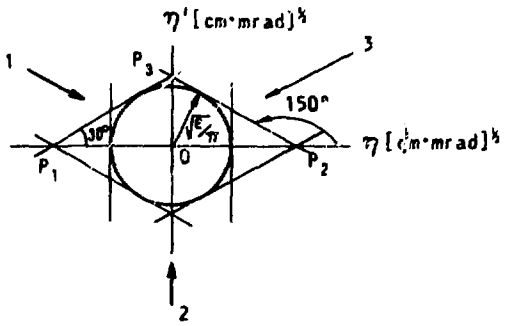

Fig. A-1.
Three equally spaced views of a beam in normalized phase space.

Thus, when the beam is drifted downstream from position 2, the tangent line pivots about y_1 until it becomes vertical. At this point the beam extent is twice as large as at the waist.

Hence, the criterion for equally spaced views is that the beam extent should be doubled on both sides of a waist. For a drift space, this means that the drift length from the waist is

$$\ell = \beta\sqrt{3} ,$$

where β is evaluated at the waist.

APPENDIX B

PROFILE ORDERING

A schematic diagram of the wire scanner used in experiments at LAMPF is shown in Fig. B-1.

In addition to the wires at 0° and 90°, three wires were added at −15°, 45°, and 105°. The spade holding the wires is driven by a stepping motor diagonally at 45° below the horizontal. As it proceeds, the current intercepted by the wires develops projection profiles of the beam on planes at −90° from the wire directional. As shown in Fig. B-2, the development of the profile proceeds in the direction shown by the arrow on each plane.

In RECON60, it is assumed that the profiles are taken 120° apart and that the ordering is counterclockwise. (See Fig. B-3.) The 135° profile then must be obtained from the −45° profile by reversing its order.

After the hexagonal grid is mapped onto a square grid, one of the directions, possibly 135°, will coincide with the matrix column direction. A final rotation of 45° counterclockwise would then have to be made for final display at the correct orientation.

In RECON45 no reordering is required. The program was made to conform to the LAMPF wire scanner apparatus. (See Fig. B-4.)

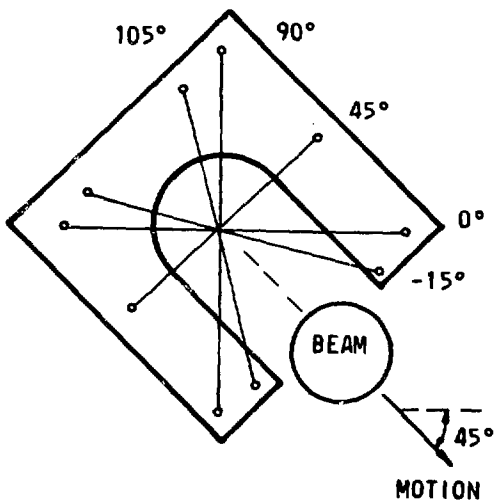

Fig. B-1.
Schematic diagram of wire scanner used in LAMPF experiments.

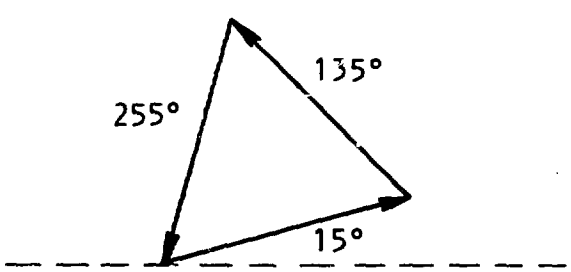

Fig. B-3.
Profile ordering for RECON60.

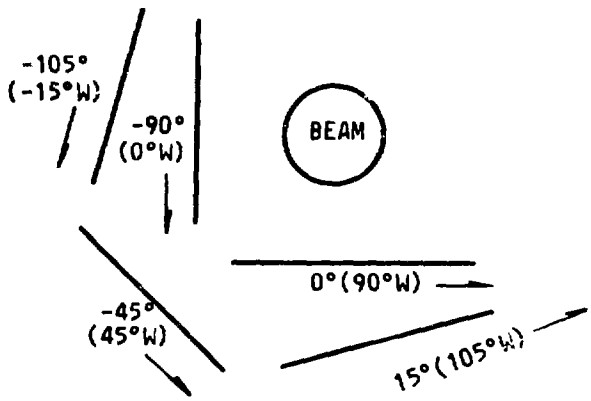

Fig. B-2.
Projection planes and profile ordering for the wire scanner of Fig. B-1. The angle of the wire on which the profile is registered is shown in parentheses.

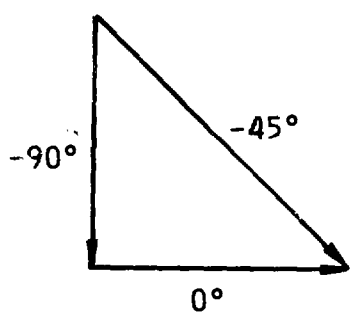

Fig. B-4.
Profile ordering for RECON45.

APPENDIX C

RECONSTRUCTION GRID FOR RECON45

Each square pixel of a square grid is bisected diagonally to form 45° isosceles triangular pixels. (See Fig. C-1.) Ray sums can then be done in all three directions without weighting. The step size for the −45° projection must be $1/\sqrt{2}$ times the horizontal and vertical step size. The center element of the −45° profile must be located so that it projects back to the center of the grid.

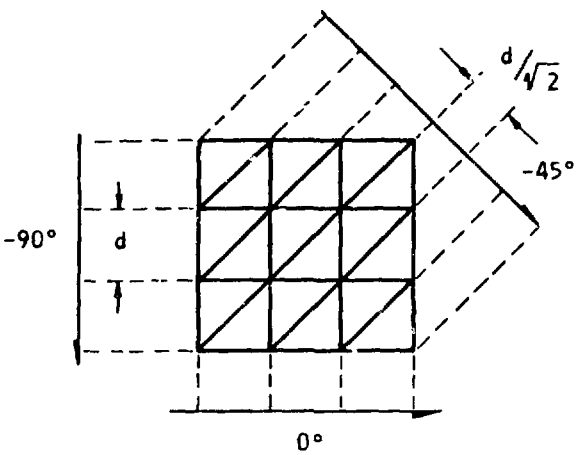

Fig. C-1.
Reconstruction grid for three projections at 0°, −45°, and −90°.

APPENDIX D

CALCULATION OF WEIGHTS IN RECONWT

A square grid is used. Rays are drawn across the grid at an angle θ for a projection plane at an angle $\theta + 90°$. (See Fig. D-1.)

The pixel weight is the fractional area of the pixel that lies between the ray boundaries. For convenience, the ray width is made equal to the width of the square pixels.

In each pixel, the area lying under the line m−1 is calculated, then the area under the line m is subtracted.

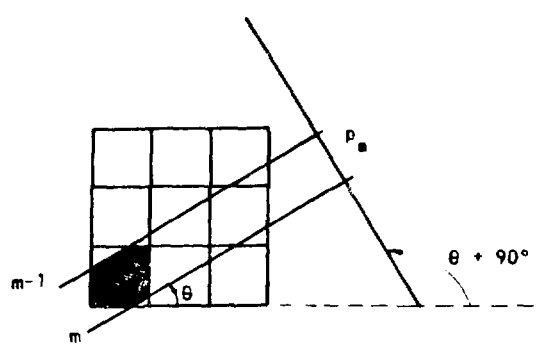

Fig. D-1.
Calculation of pixel weight in a projection ray.

APPENDIX E

GENERAL LINEAR TRANSFORMATION OF A SQUARE PIXEL

In the RECON program, an arbitrary linear transformation of two variables is used. A square pixel is mapped into a quadrilateral by the transformation. (See Fig. E-1.) The fractional areas of all square pixels intersected by the transformed old pixel are calculated. The density in the old pixel is distributed among all the intersected pixels in proportion to the corresponding fractional weight.

The procedure is as follows: first, the location of the four corners of the transformed pixel are calculated. Then the corners are ordered in counterclockwise order with the leftmost corner numbered one. A buffer matrix is defined such that the old pixel is just enclosed in it. The buffer matrix corresponds to the subset of pixels intersected by the quadrilateral. To calculate the fractional overlap areas of the pixels within the buffer matrix, it is useful to classify the quadrilateral shapes according to whether the third, second, or fourth apex is at the extreme right of the buffer. (See Fig. E-2.) With this classification partial areas are computed as follows for each pixel within the buffer matrix.

Class 1: Compute areas above lines 12 and 23. Subtract areas above lines 34 and 41.

Class 2: Compute areas above line 12. Subtract areas under lines 23, 34, and 41.

Class 3: Compute areas above lines 12, 23, and 34. Subtract areas above line 41.

The fractional areas computed in the buffer matrix are then added to the corresponding pixels in the reconstruction grid.

A useful check on the mapping calculation is the sum of the fractional areas in the buffer. For a rotational transformation, the buffer size is not larger than 3 by 3. In this case the sum of the fractional areas has been determined at $1 \pm 1 \times 10^{-12}$. Another check sum is the total density in the reconstruction area after a number of mapping cycles. In a typical case the total density has been ascertained constant within 1 part in 10.

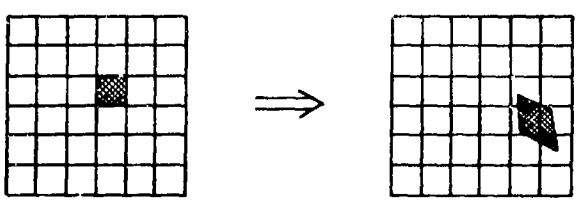

Fig. E-1.
Mapping of a square pixel to a quadrilateral pixel by a linear transformation.

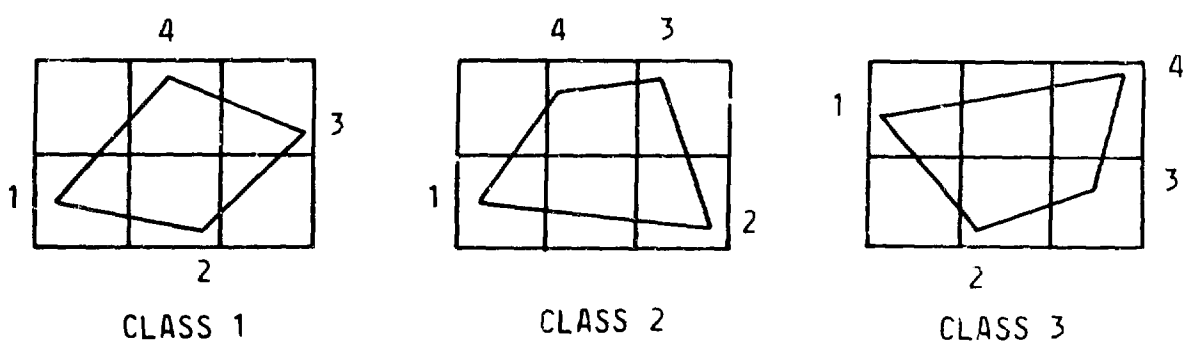

Fig. E-2.
The three classes of quadrilaterals within a buffer matrix.